

Cite this: *J. Mater. Chem. B*, 2018,
6, 7750

Overcoming drug resistance with functional mesoporous titanium dioxide nanoparticles combining targeting, drug delivery and photodynamic therapy†

Zhaoming Guo,^a Kun Zheng,^a Zhenquan Tan,^b Ye Liu,^a Ziyin Zhao,^a
Guang Zhu,^a Kun Ma,^a Changhao Cui,^a Li Wang^a and Tianyu Kang^a

The resistance of tumor cells is a major cause of chemotherapy failure in cancer patients. Photodynamic therapy (PDT) as a noninvasive treatment strategy with high specificity is a promising method for the treatment of cancer. In this study, a CD44 and N-cadherin dual targeting drug delivery system in combination with mesoporous titanium dioxide nanoparticle (MTN)-based PDT has been successfully constructed for overcoming drug resistance. Hyaluronic acid (HA) and ADH-1 (a cyclic pentapeptide) were grafted onto the surface of MTN to construct ADH-1-HA-MTN, and doxorubicin (DOX) was selected as a model drug. HA can both trap DOX in the wells of MTN and target CD44-overexpressing tumor cells. ADH-1 blocks the EMT process of tumor cells by selectively inhibiting the function of N-cadherin. Besides, a large number of reactive oxygen species (ROS) were generated by MTN under X-ray irradiation, which could provide a cancer cell killing effect. Cytotoxicity tests showed that ADH-1-HA-MTN/DOX was more toxic to tumor cells than its non-ADH-1 modified counterparts. Western blotting analysis showed that ADH-1-HA-MTN/DOX overcame the drug resistance of tumor cells by preventing the process of epithelial–mesenchymal transition. Taken together, ADH-1-HA-MTN may be a promising targeted drug delivery system to overcome the drug resistance of tumors.

Received 11th July 2018,
Accepted 16th October 2018

DOI: 10.1039/c8tb01810c

rsc.li/materials-b

Introduction

Malignant tumors are worldwide threats to human health, and a lot of people die of cancer every year. Until now, chemotherapy has been and is still the main strategy for cancer treatment. However, the success of chemotherapy is usually frustrated by the development of drug resistance. Such acquired resistance of tumor cells is reported to be largely attributable to the cell-biological process termed epithelial-to-mesenchymal transition (EMT).^{1,2}

During EMT, cells lose their polarity and epithelial cell–cell junctions, resulting in their disassociation from epithelial sheets. Meanwhile, they acquire mesenchymal properties, including acquisition of motility capacity and heightened resistance to apoptosis as well as the ability to degrade and reorganize the extracellular matrix.^{3–6} When EMT occurs in tumor cells, multiple apoptotic signalling pathways are downregulated and drug efflux is enhanced, contributing to the enhanced resistance

of tumor cells to anticancer drugs. Therefore, it offers a potential avenue for overcoming drug resistance to selectively target tumor cells that have undergone EMT.

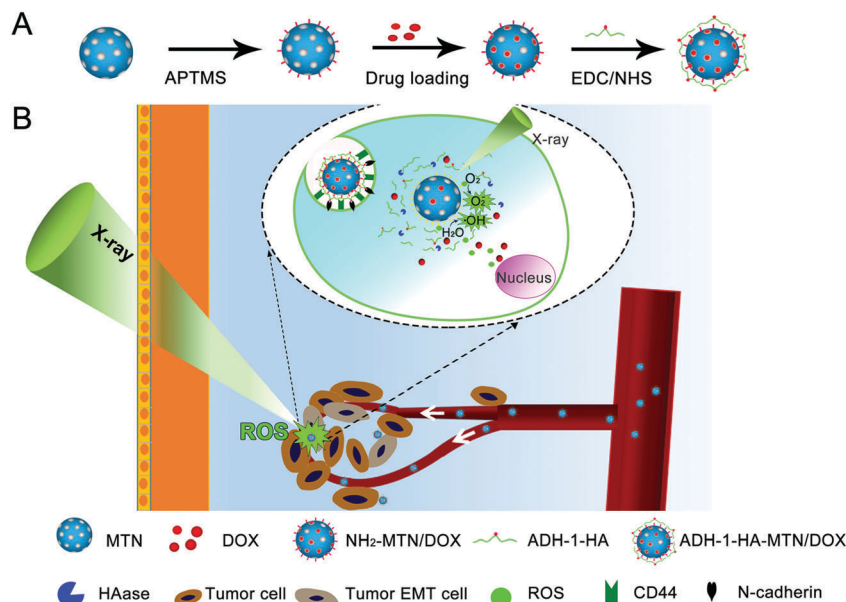
N-cadherin, an important marker of EMT, is expressed on the cell surface of the EMT cells.⁷ Hence, N-cadherin is an ideal target for EMT targeting treatment.⁸ The cyclic pentapeptide ADH-1, an antagonist of N-cadherin, is used here to selectively block the function of N-cadherin.⁹

In recent years, reactive oxygen species (ROS)-mediated cancer therapies such as photodynamic therapy (PDT) have gained much attention because of their minimal invasiveness, site-specific activation, and well-established clinical applications.^{10,11} PDT uses light to activate a photosensitizer to generate ROS, which induces direct cancer cell death.¹² Mesoporous titanium dioxide nanoparticles (MTNs), just like other mesoporous nanoparticles such as mesoporous silica (MSN), with low cytotoxicity and suitable drug loading pore size have been studied for use as drug delivery systems. In addition, the advantage of MTN is that TiO₂ nanoparticles could absorb ultraviolet (UV) light and generate ROS while MSN itself could not be activated by an external stimulus and could not play a therapeutic role in cancer treatment.^{13–17} Hence, different from MSNs, TiO₂ nanoparticles can be used for PDT. Although UV-activated TiO₂ NPs have very good prospects, this strategy appears to be ineffective in treating

^a School of Life Science and Medicine, Dalian University of Technology, Panjin, Liaoning, 124221, China. E-mail: guozm@dlut.edu.cn; Fax: +86-427-2631889; Tel: +86-427-2631427

^b School of Petroleum and Chemical Engineering, Dalian University of Technology, Panjin, Liaoning, 124221, China

† Electronic supplementary information (ESI) available. See DOI: 10.1039/c8tb01810c



Scheme 1 (A) Schematic illustration of the preparation of ADH-1-HA-MTN/DOX. (B) Schematic illustration of ADH-1-HA-MTN/DOX for CD44 and N-cadherin dual targeting drug delivery and the photodynamic effect upon X-ray irradiation.

some kinds of cancers and is difficult to clinically apply for two major reasons. First, ultraviolet penetration depth is a major obstacle that limits the technique's use to surface cancers such as skin cancer, nasopharyngeal cancer, and oral cancer.^{18,19} Second, the UV-mediated ROS production lasts for a very short time and is not enough to provide a continuous and prolonged cancer-killing effect.²⁰ However, the use of X-rays to irradiate MTN to produce ROS can effectively avoid the above two problems.

In this work, unlike recent studies on MTN nanocarriers, we presented a strategy in which a MTN-based drug delivery system could overcome the drug resistance of tumor cells by EMT targeting chemotherapy combined with PDT. For the proof of concept, we designed a nano-drug delivery system ADH-1-HA-MTN. As shown in Scheme 1, MTNs were used as the drug delivery carriers and doxorubicin (DOX) was chosen as the model drug. HA acted as an active targeting ligand to achieve targeted drug delivery to CD44-overexpressing tumor cells and a cross-linking molecule to conjugate ADH-1 on the surface of the MTN. ADH-1 acted as an antagonist to block the function of N-cadherin, thus preventing the EMT process. We hypothesized that ADH-1-HA-MTN/DOX can overcome the drug resistance of tumor cells by the following steps: first, the drug delivery system can be specifically recognized by tumor cells *via* the crosstalk between HA and CD44.²¹ Second, ADH-1 inhibits the EMT process of tumor cells by blocking the function of N-cadherin. Finally, encapsulated DOX and X-ray stimulation of MTN-generated ROS further kill the tumor cells.

Experimental section

Materials

(3-Aminopropyl)trimethoxysilane (APTMS) was purchased from Macklin. Titanium butoxide (GC, 99.0%), heptanoic acid (AR, 98.0%), ethanol, *N*-(3-dimethylaminopropyl)-*N*-ethylcarbodiimide

hydrochloride (EDC), *N*-hydroxysuccinimide (NHS) and doxorubicin hydrochloride (DOX) were purchased from Aladdin (Shanghai, China). Sodium hyaluronate (molecular weight, 37 kDa) was purchased from Freda (Shandong, People's Republic of China). 4',6-Diamidino-2-phenylindole (DAPI) was obtained from Solarbio (Beijing, China). Cell Counting Kit-8 (CCK-8) was purchased from Beyotime. Foetal bovine serum (FBS), RPMI 1640, trypsin-EDTA and penicillin-streptomycin were obtained from HyClone. The ADH-1 peptide (N-AC-CHAVC-NH₂) was obtained from GL Biochem Peptide Ltd. (Shanghai, China). DCFH-DA was purchased from Beyotime. The calcein-AM/PI double staining kit was obtained from Dojindo (Beijing, China). RIPA lysis buffer, PMSF and the enhanced chemiluminescence kit were purchased from Coolaber Science & Technology Co., Ltd. The BCA kit was obtained from Solarbio Science & Technology Co., Ltd. (Beijing, China). All antibodies were obtained from Biodragon-immunotech (Beijing, China).

Preparation of NH₂-MTN

MTNs were synthesized according to a published method.²² Briefly, 5 μ L of heptanoic acid was added into 20 ml of ethanol under stirring for 20 minutes. Then 300 μ L of tetrabutyl titanate was added with stirring for another 15 minutes. 5 mL of ultrapure water was added into the solution and stirred for half an hour. Finally the hydrothermal reaction was conducted at 120 $^{\circ}$ C. The resulting product was centrifuged, and washed successively with ethanol and ultrapure water three times.

For the synthesis of NH₂-MTN, 2 mg of MTN was dissolved in 25 mL of ethanol. The mixture was sonicated to disperse uniformly. 50 μ L of APTMS was added to the mixture and stirred for 24 hours at room temperature. The reaction product was then washed successively with ethanol and ultrapure water three times and dispersed in ultrapure water for preservation.

Synthesis of ADH-1-HA-MTN

10 mg of NH₂-MTN was dissolved in 4 mL of PBS solution (pH 6.5) and sonicated to disperse well. Then, 4 mg of DOX was added to the mixture and stirred at room temperature for 24 h in the dark to obtain the DOX-loaded NH₂-MTN (NH₂-MTN/DOX). The nanoparticles were centrifuged, washed with PBS (pH 6.5) three times, and analyzed using an Ultraviolet-visible (UV-vis) spectrometer to verify the successful loading of DOX. Then, 2.5 mg of ADH-1-HA was hydrated for 24 h, followed by activation with EDC and NHS for 2 h. 10 mg of NH₂-MTN/DOX was added to the activated ADH-1-HA solution and stirred for 12 h. The resulting nanoparticles were washed with PBS (pH 7.4) three times and stored in PBS for further use.

In vitro drug release

The *in vitro* release behavior of DOX from nanoparticles (MTN/DOX, HA-MTN/DOX or ADH-1-HA-MTN/DOX) was studied using a dialysis method. Briefly, nanoparticles were suspended in PBS of two different pH values (5.0 and 7.4), respectively. The concentration of the nanoparticles was 1 mg mL⁻¹. Then, the mixture was placed in a dialysis bag (*M_w* = 14 000) and the release medium was equilibrated with 60 mL of the corresponding PBS buffer at 37 °C under horizontal shaking (100 rpm). 200 μL of the solution was withdrawn from the buffer medium and replaced with an equal volume of fresh medium at predetermined time points. The amount of released DOX was measured using a microplate reader (BioTek, USA) at an excitation wavelength of 480 nm and emission wavelength of 587 nm. In addition, HAase was added to degrade the modified HA on the surface of ADH-1-HA-MTN/DOX.

Characterization

The particle size, potentials and polydispersity (PDI) of the synthesized MTN, NH₂-MTN, HA-MTN and ADH-1-HA-MTN were measured by dynamic light scattering (DLS) analysis using a Malvern Zetasizer Nano ZS (Malvern, UK). Scanning electron microscopy (FE-SEM, Nova NanoSEM 450) was used to observe the morphology of the above nanoparticles. Transmission electron microscopy (TEM) was carried out using an FEI Tecnai G2 F30 instrument equipped with EDX (Bruker super-X). Nitrogen adsorption-desorption measurements were carried out in a liquid nitrogen atmosphere and samples were outgassed for 6 h before the measurements were taken. The surface area and pore size distribution of the samples were measured by Brunauer Emmett Teller (BET) and Barrett Joyner Halenda (BJH) measurements. FT-IR spectra were measured using a Fourier transform infrared spectrometer (FT-IR, Nicolet iN10 MX & iS10, ThermoFisher) with KBr pellets. Thermogravimetric analysis (TGA) was carried out on a Mettler Toledo TGA/DSC1 instrument. ¹H NMR spectra were recorded on a Bruker AVANCE III HD 500 MHz using deuterium oxide (D₂O) as the solvent. An ultraviolet-visible (UV-vis) spectrometer (Thermo Scientific Instrument Co., Ltd) was used to analyze the content of DOX.

Hemolysis assay

Fresh blood was obtained from rabbit ear marginal veins and red blood cells (RBCs) were isolated by centrifugation at

1000 rpm for 20 minutes at 4 °C. Then, RBCs were washed three times with PBS until the supernatant was clear. 1 mL of the nanoparticle (MTN, HA-MTN or ADH-1-HA-MTN) suspension in PBS at different concentrations was placed in centrifuge tubes. Deionized water was used as the positive control and saline was used as the negative control. After 0.5 h of incubation in the water bath at 37 °C, 0.1 mL of the RBC suspension was added. Following 2 h of incubation at 37 °C under constant shaking, the suspensions were centrifuged at 1000 rpm for 10 min. The color of the supernatant in each centrifuge tube was observed to determine the hemolytic phenomenon. Then, 200 μL of the supernatant from each tube was added into a 96-well plate. The absorbance (OD value) of each sample was measured using a microplate reader at a wavelength of 576 nm. The hemolysis percentage was calculated using the following equation:

$$\text{Hemolysis (\%)} = \frac{(\text{OD}_{576} \text{ sample} - \text{OD}_{576} \text{ negative control})}{(\text{OD}_{576} \text{ positive control} - \text{OD}_{576} \text{ negative control})} \times 100\%$$

Cell culture

The A549 human non-small cell lung carcinoma cell line was purchased from the Institute of Basic Medical Science, Chinese Academy of Medical Sciences (Beijing, China). Cells were incubated in complete RPMI 1640 (RPMI 1640 with 10% (v/v) FBS and 100 U mL⁻¹ of penicillin and streptomycin) at 37 °C in a humidified atmosphere containing 5% CO₂.

Establishment of the EMT cell model

A549 cells of 30–40% confluence were cultured in serum-free RPMI medium for 24 hours. Then, cells were stimulated with 5 ng mL⁻¹ TGF-β1 for 48 h.

Cellular uptake assay

The cellular uptake of nanoparticles (MTN/DOX, HA-MTN/DOX or ADH-1-HA-MTN/DOX) by A549/EMT cells was evaluated by confocal imaging. For confocal imaging, cells were seeded in 24-well plates and incubated for 24 h. Then, cells were incubated in a medium containing MTN/DOX, HA-MTN/DOX, ADH-1-HA-MTN/DOX or free DOX at a final DOX concentration of 10 μg mL⁻¹. For the receptor blocking study, cells were pre-incubated with free HA (2 mg mL⁻¹) for 1 h prior to the addition of ADH-1-HA-MTN/DOX. After 3 h of incubation, cells were washed three times with cold PBS and fixed with 4% paraformaldehyde. The nuclei were stained with DAPI (10 ng mL⁻¹). Finally, the cells were imaged under a laser confocal fluorescence microscope (LSCM, Leica, TCS SP8, Germany). To compare the cellular uptake of different nanoparticles quantitatively, flow cytometry analysis was carried out. Cells were seeded in 12-well plates and incubated for 24 h. Then, cells were incubated in a serum-free medium containing different DOX formulations at a final DOX concentration of 10 μg mL⁻¹. For the receptor blocking study, cells were pre-incubated with free HA (2 mg mL⁻¹) for 1 h prior to the addition of ADH-1-HA-MTN/DOX. After 3 h of incubation, the cells were washed with cold PBS, then detached by trypsinization and suspended in 400 μL of PBS.

The samples were analysed by flow cytometry using a FACScan flow cytometer (Becton Dickinson FACSCalibur, USA).

Detection of intracellular ROS generated by MTNs under X-ray irradiation

Intracellular ROS produced upon X-ray irradiation were detected using a DCFH-DA Reactive Oxygen Species Assay Kit. Approximately 5×10^4 A549 cells per well were seeded in six-well plates. After incubation with MTN, HA-MTN, HA-ADH-1-MTN ($10 \mu\text{g mL}^{-1}$) for 24 h, DCFH-DA was added and incubated for another 1 h. Then, the cells were washed twice with PBS and exposed to X-rays for 0.5 h. X-ray irradiation was performed using a BJI-1 (Xianwei, Shanghai, China) at a voltage of 60–75 kV and a current of 0.15–0.35 mA. After another 0.5 h of incubation, fluorescence images of the treated cells were acquired using an inverted fluorescence microscope (Leica DMI4000B). For flow cytometry analysis, cells were treated the same way as above. Finally, cells were detached by trypsinization and suspended in 400 μL of PBS. The samples were analysed by flow cytometry using a FACScan flow cytometer (Becton Dickinson FACSCalibur, USA).

Evaluation on therapeutic effects of PDT *in vitro*

To evaluate the photodynamic effect of the nanoparticles, A549/EMT cells were seeded in 24-well plates at a density of 5×10^4 cells per well. After 24 h of incubation, cells were incubated with different nanoparticles (MTN, HA-MTN or ADH-1-HA-MTN) followed by X-ray irradiation for 30 minutes. X-ray irradiation was performed using a BJI-1 (Xianwei, Shanghai, China) at a voltage of 60–75 kV and a current of 0.15–0.35 mA. Then, 5 mL of Calcein-AM (2 mM) and 15 μL of PI (1.5 mM) were added into each well. After incubation for another 30 minutes, fluorescence images of the treated cells were acquired using an inverted fluorescence microscope (Leica DMI4000B). Quantitative results of live/dead cells were measured by counting green fluorescence stained cells and red fluorescence stained cells using imageJ software.

In vitro cytotoxicity assay

For *in vitro* cytotoxicity assay, A549 cells or A549/EMT cells were seeded in 96-well plates at a density of 5×10^3 cells per well and incubated overnight. Then, cells were treated with different nanoparticles (MTN, HA-MTN or ADH-1-HA-MTN) or DOX-loaded groups (DOX, MTN/DOX, HA-MTN/DOX or ADH-1-HA-MTN/DOX), with or without X-ray irradiation for 30 minutes. After another 24 h of incubation, 10 μL of CCK-8 was added to each well. The cells were incubated for 1 h at 37 °C and the absorbance was determined using a microplate reader (BioTek, USA) at 450 nm.

Western blotting assay

Western blotting was performed to study the change of the protein expression. Cells treated with different formulations were lysed in RIPA Lysis Buffer and PMSF cocktail (1 mM). Then, lysates were centrifuged at 12 000 g min^{-1} for 5 min and supernatants were collected. The proteins were quantitated

using the BCA kit, separated by SDS-polyacrylamide gels and then transferred to PVDF membranes. The PVDF membranes were incubated with the indicated primary antibody at 4 °C overnight. Then, the membranes were incubated with HRP Conjugated Polyclonal Goat Anti-Rabbit IgG (H + L) (1 : 8000) for 2 h at room temperature. Finally, the immune complexes were treated with an enhanced chemiluminescence kit and imaged using a sensitive chemiluminescent imaging system (FluoChem HD2, Protein Simple, USA).

Statistical analysis

All experiments were repeated at least three times. All the quantitative data are shown as mean \pm SD. Student's *t*-test was used to determine statistical significance ($*p < 0.05$; $**p < 0.01$).

Results and discussion

Synthesis and characterization of functionalized MTN

The synthesis of ADH-1-HA-MTN/DOX was divided into four steps. (1) The MTNs were synthesized according to a published method.²² (2) MTNs were modified with APTMS to synthesize NH_2 -MTN. (3) DOX was loaded into the NH_2 -MTN by diffusion in an aqueous medium under mechanical agitation. (4) The amino group in NH_2 -MTN/DOX was conjugated with the carboxyl group in ADH-1-HA through an amide bond to form ADH-1-HA-MTN/DOX. It is worth noting that ADH-1-HA used here was previously synthesized and characterized by our research group for subsequent experiments,⁸ and the synthesis pathway is shown in Fig. S1 (ESI[†]).

The morphology, particle size, and zeta potential properties of the functionalized MTNs were characterized. As shown in Fig. 1A, the synthesized ADH-1-HA-MTN measured by DLS had a particle size of approximately 100 nm. Investigations confirmed that nanoparticles < 200 nm in diameter could circulate in blood for an extended period and accumulate in the tumor site.²³ Thus, our developed ADH-1-HA-MTN might be a useful carrier for tumor targeted drug delivery. With the modification of different materials, the zeta potential greatly changed, indicating the successful modification (Fig. 1B). The morphology of MTN, HA-MTN and ADH-1-HA-MTN was spherical and relatively uniform in SEM images and all of the nanoparticles showed a highly porous structure in TEM images (Fig. 1C). Then, elemental analysis was performed on ADH-1-HA-MTN. As shown in Fig. 1D, the S element could be found in the energy spectrum of ADH-1-HA-MTN. This result proved that ADH-1-HA was successfully grafted onto the surface of the MTN because only ADH-1 contains the S element.

Then, the successful construction of ADH-1-HA-MTN was further validated by Fourier transform infrared (FTIR) spectra. As shown in Fig. 2A, compared with MTN, the emerging amino group absorption peak at 1506 cm^{-1} suggested the successful synthesis of NH_2 -MTN. The absorption peaks of C=O were found at 1732 cm^{-1} , which proved the successful synthesis of HA-MTN. For ADH-1-HA-MTN, absorption peaks at 1645 cm^{-1} and 539 cm^{-1} (C=C and S-S stretching vibrations of the five-membered

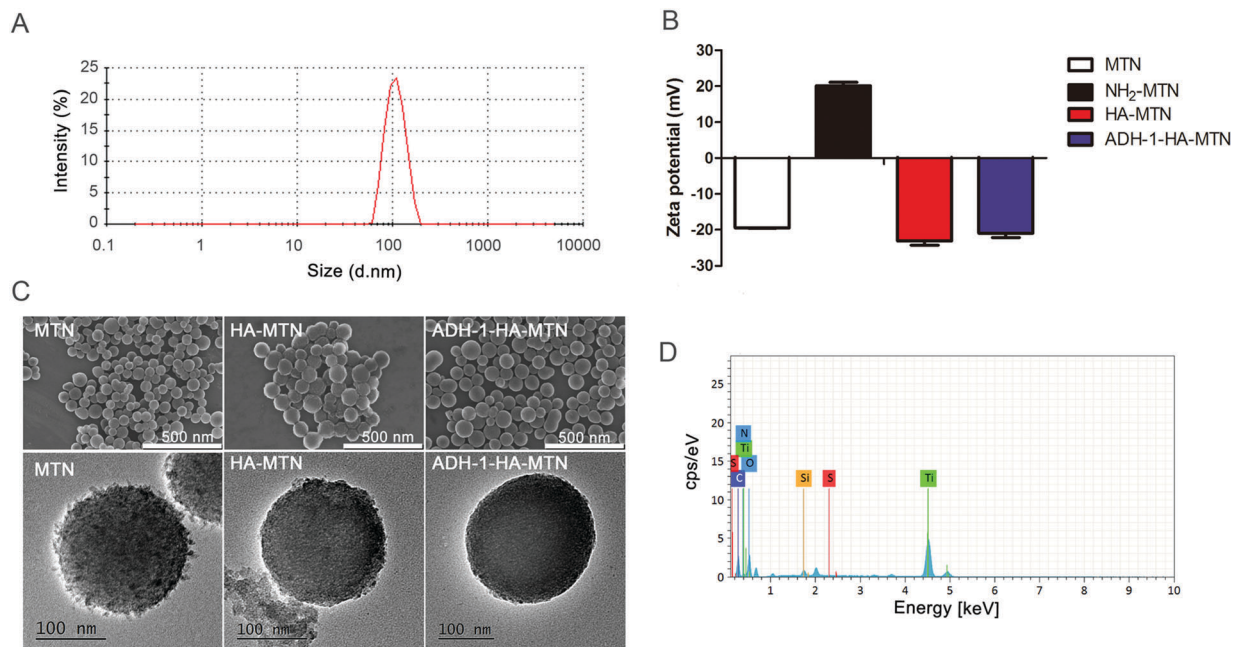


Fig. 1 (A) Size distribution of ADH-1-HA-MTN. (B) Zeta potentials of MTN, NH_2 -MTN, HA-MTN and ADH-1-HA-MTN. (C) SEM micrographs (upper panel) and TEM micrographs (lower panel) of MTN, HA-MTN and ADH-1-HA-MTN. (D) Energy spectrum analysis of ADH-1-HA-MTN.

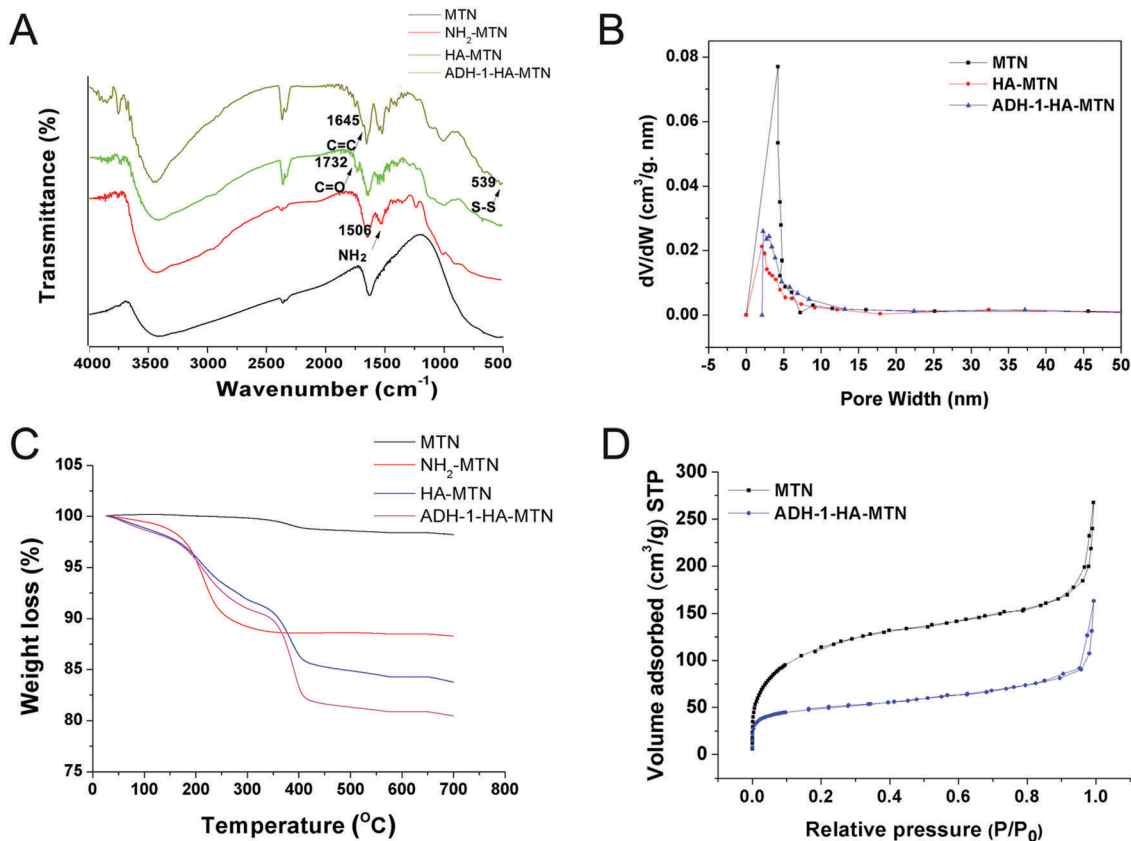


Fig. 2 (A) FT-IR spectroscopy of MTN, NH_2 -MTN, HA-MTN and ADH-1-HA-MTN. (B) Pore size distribution of MTN, HA-MTN and ADH-1-HA-MTN from BJH adsorption. (C) TGA curves of NH_2 -MTN, HA-MTN and ADH-1-HA-MTN. (D) The nitrogen adsorption/desorption isotherms of MTN and ADH-1-HA-MTN.

heterocycle in ADH-1, respectively) were observed, indicating the successful construction of ADH-1-HA-MTN. Besides, the pore size of the original MTN was 4 nm, while the pore size of HA-MTN or ADH-1-HA-MTN decreased to about 2 nm (Fig. 2B). The results indicated that MTN was coated with HA or ADH-1-HA. The TGA profiles demonstrated that the weight loss of NH₂-MTN, HA-MTN, and ADH-1-HA-MTN was 9.93%, 13.75% and 17.76%, respectively. These results manifested that the weight percentage of ADH-1-HA in ADH-1-HA-MTN was 7.83% (Fig. 2C). The nitrogen adsorption/desorption isotherms and pore size distribution curves of MTN and ADH-1-HA-MTN are shown in Fig. 2D. The two samples showed type IV isotherms, further indicating the mesoporous structure of the nanoparticles. The monolayer adsorption capacities of MTN and ADH-1-HA-MTN were 136.7 mL and 37.2 mL, respectively.

Drug loading and pH-responsive drug release

As shown in Fig. S2 (ESI[†]), the absorption peak of MTN/DOX was seen at 480 nm, the same as that of DOX measured by UV-vis spectroscopy. This result demonstrated that DOX was indeed loaded into MTN. The DOX loading content and encapsulation efficiency were 25.4% and 96.7%, respectively. Then, MTN/DOX was modified with HA or ADH-1-HA as described previously to synthesize HA-MTN/DOX and ADH-1-HA-MTN/DOX. Fig. 3 shows the drug release curves of MTN/DOX, HA-MTN/DOX and ADH-1-HA-MTN/DOX. All three groups demonstrated sustained drug release behavior. At pH 7.4, the drug release from the delivery systems was mainly by a passive leakage and the cumulative amount of drug released was less than 40% (Fig. 3A). This might intrinsically render the drug delivery systems weaker than those based purely on a pH-triggered release which could overcome the limitations of chemotherapy. However, the cumulative amount of drug released was greater at pH 5.0 than that under simulated physiological conditions (PBS, pH 7.4) (Fig. 3B). This suggested that the synthesized nanocarriers exhibited pH-dependent drug release properties. This will be more conducive for drug-loaded nanocarriers to achieve drug release in tumor cells. In addition, it could be found from Fig. 3 that the DOX release amount of HA-MTN/DOX or ADH-1-HA-MTN/DOX was lower than that of MTN/DOX. This could be due to the HA or ADH-1-HA coated on MTN. As a result, DOX in the pores of MTN could not be effectively released. However, the DOX released from HA-MTN/DOX or ADH-1-HA-MTN/DOX was markedly increased when HAase was added. This was because the HA on the surface of HA-MTN/DOX or ADH-1-HA-MTN/DOX was degraded by HAase,²⁴ resulting in the release of DOX from the pores.

Toxicity studies

Hemolysis (damage to red blood cells (RBCs)) is a fundamental *in vitro* test to determine the safety of a blood-contacting nanomaterial.^{25,26} Fig. 4A shows the hemolysis results caused by the exposure of MTN, HA-MTN or ADH-1-HA-MTN to diluted rabbit blood. There was no obvious hemolysis in the nanoparticle-containing groups. The percent of hemolysis remained below 3% across all the concentration ranges tested (Fig. 4B). According to the ASTM E2524-08 standard, a hemolysis percent less than 5% indicates that the test material is non-hemolytic.²⁷

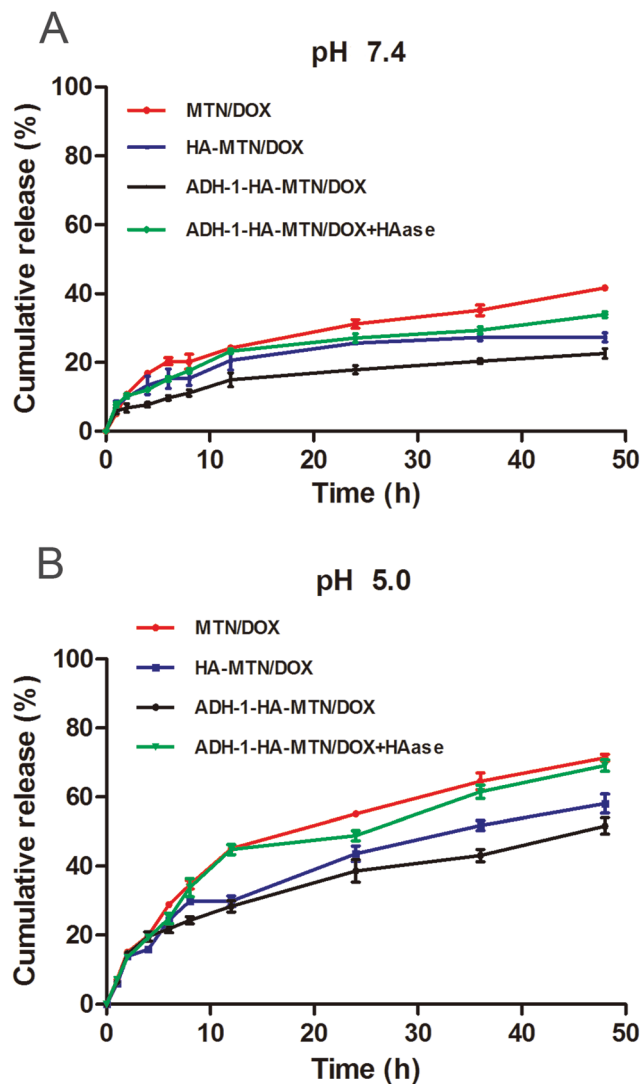


Fig. 3 The cumulative release of DOX from MTN/DOX, HA-MTN/DOX or ADH-1-HA-MTN/DOX at (A) pH 7.4 and (B) pH 5.0. Data are presented as mean \pm SD ($n = 3$).

Establishment and verification of the EMT cell model

The establishment of the EMT cell model was conducted using a previous method.⁸ Briefly, A549 lung cancer cells were cultured with TGF- β 1 (5 ng mL⁻¹) for 48 h to establish A549/EMT cells.^{28–30} Fig. 5 shows the western blotting results consistent with the EMT change including the increase of N-cadherin and Snail, and the decrease of E-cadherin expression. These results suggested that A549/EMT had been successfully established. Furthermore, the IC₅₀ values of DOX for A549 cells and A549/EMT cells were 0.7 μ g mL⁻¹ and 1.35 μ g mL⁻¹, respectively. The resistance index was close to 2. This result proved that the cells that have undergone EMT developed drug resistance.

In vitro cellular uptake studies

In order to assess the targeting ability of ADH-1-HA-MTN/DOX, cellular uptake studies were performed on A549/EMT cells. The extent of the internalization of DOX or DOX loaded

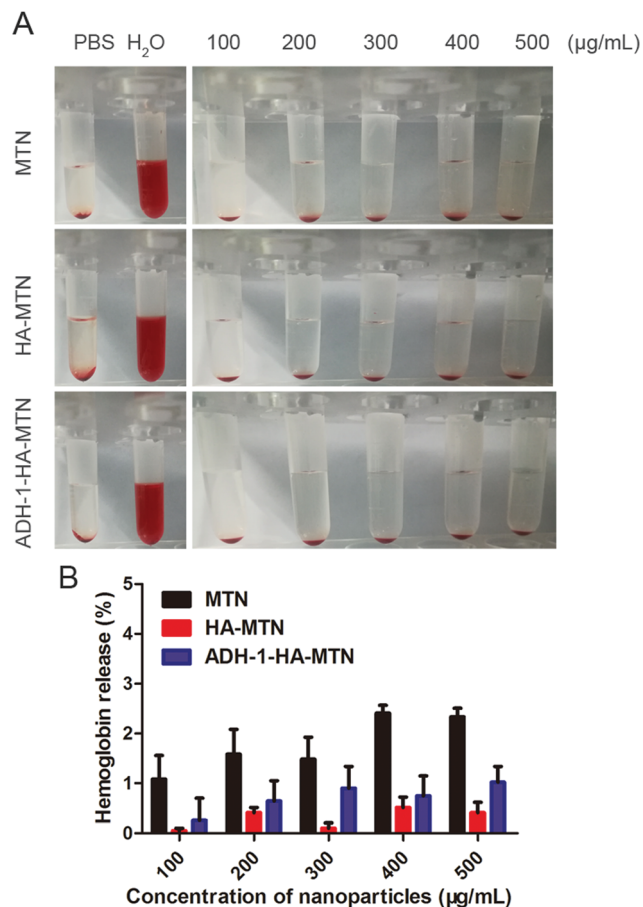


Fig. 4 (A) Hemolysis study for MTN, HA-MTN and ADH-1-HA-MTN. (B) The hemolysis rate in RBCs upon 2 h incubation with different nanoparticles at incremental concentrations, data are mean \pm SD ($n = 3$).

nanoparticles into A549/EMT cells was investigated by laser confocal microscopy. The red fluorescence in Fig. 6A indicates the distribution of DOX loaded nanoparticles in the cells and blue fluorescence indicates the nuclei stained by DAPI. Cells exposed to free DOX showed the highest fluorescence intensity in the nucleus. This is due to the fact that the intracellular DOX molecules in the cytoplasm can rapidly transmit to the nucleus and bind tightly to the chromosomal DNA.^{24,31} For ADH-1-HA-MTN/DOX and

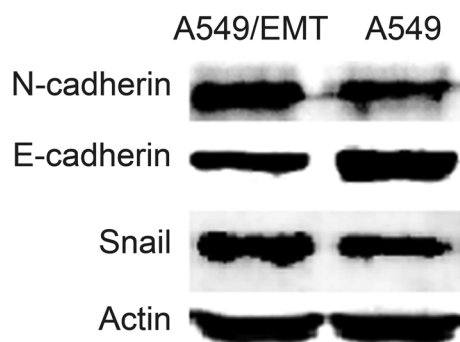


Fig. 5 The expression of epithelial phenotype markers and mesenchymal markers in A549 cells and TGF- β_1 -stimulated A549 cells (A549/EMT).

HA-MTN/DOX groups, the fluorescence intensity was much stronger than that of the MTN/DOX group, indicating that ADH-1-HA-MTN/DOX and HA-MTN/DOX were internalized much more rapidly and efficiently by A549/EMT cells within 3 h of incubation. To further investigate the targeting role of HA in the cellular uptake of ADH-1-HA-MTN/DOX, we conducted a receptor competition assay. After the pre-incubation of free HA, the cellular fluorescence intensity was significantly decreased in the ADH-1-HA-MTN/DOX group. Quantitative analysis by flow cytometry also demonstrated a similar result. These results suggested that HA modified on the nanoparticles could trigger CD44 mediated endocytosis.

Intracellular ROS generated by different MTNs under X-ray irradiation

In this study, MTNs are not only used as a drug carrier, but more importantly they can also kill tumor cells with their photodynamic effect. The intracellular ROS was detected using a DCFH-DA fluorescent probe. The result is shown in Fig. 7A. In the X-ray groups, we observed a distinct green fluorescence in the MTN, HA-MTN, and ADH-1-HA-MTN groups, indicating that under X-ray irradiation, the nanomaterial itself produced ROS, so as to achieve the killing effect on tumor cells. Compared with the MTN group, the green fluorescence in the HA-MTN and ADH-1-HA-MTN groups significantly increased. This was mainly due to the greater uptake of HA-MTN and ADH-1-HA-MTN by A549/EMT cells. Fig. 7B shows the results of flow cytometry analysis. The level of ROS in the cells is significantly increased after X-ray irradiation.

The therapeutic effect of PDT of different MTNs *in vitro*

We further investigated whether the produced ROS could kill tumor cells. We used the calcein-AM/PI double staining kit to detect cell survival. Calcein (green) has extremely low cytotoxicity and is used to stain live cells. PI (red) can only penetrate the dead cell membrane to reach the nucleus. As shown in Fig. 8A, there was a clear, high-intensity green fluorescence observed in the four groups without X-ray irradiation. This suggested that there was no obvious necrosis or apoptosis in the cells and the synthesized nanomaterials were safe. However, in the presence of X-irradiation, the green fluorescence in the nanomaterial-containing groups was significantly attenuated and the red fluorescence was enhanced, indicating that modified and unmodified MTN will generate ROS to induce cell death under X-ray irradiation. The quantitative result (Fig. 8B) was in accordance with the results above, further illustrating the therapeutic effect of PDT of ADH-1-HA-MTN under X-ray irradiation.

Enhanced cytotoxicity of ADH-1-HA-MTN/DOX in A549/EMT cells

The cell viability of the A549/EMT cells was assessed using Cell Counting Kit-8 assay to investigate the cytotoxicity of the nanoparticles and DOX-loaded nanoparticles. Due to the characteristics of MTN, the cytotoxicity experiments were divided into X-ray irradiation groups and non-X-ray irradiation groups. The materials themselves were verified to be non-cytotoxic (Fig. S3, ESI[†]) and the time duration of X-ray irradiation did

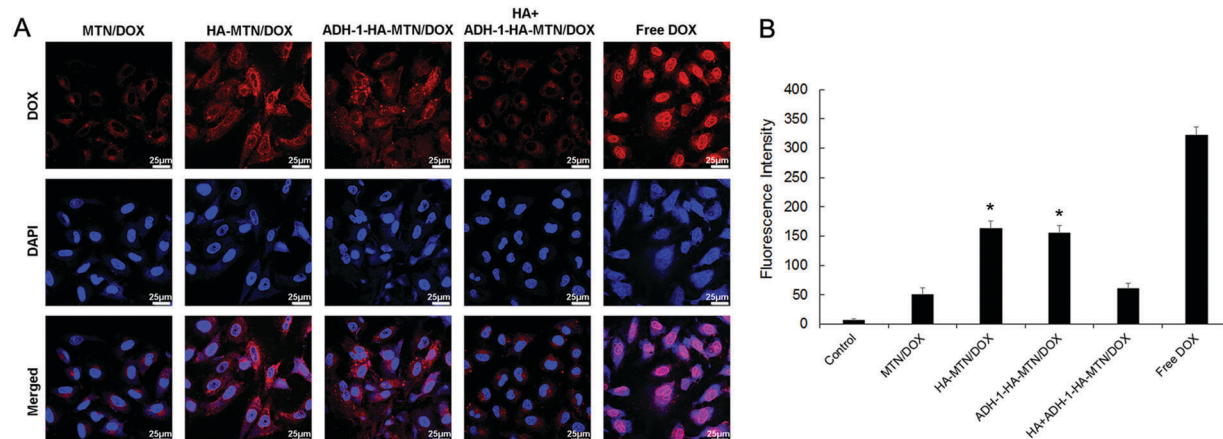


Fig. 6 (A) Confocal laser-scanning microscopy images and (B) flow cytometry quantitative results of A549/EMT cells after incubation at 37 °C for 3 h with free DOX, MTN/DOX, HA-MTN/DOX, ADH-1-HA-MTN/DOX or ADH-1-HA-MTN/DOX pre-incubated with free HA for 1 h. Data are presented as mean \pm SD ($n = 3$). * $p < 0.05$, versus MTN/DOX or MTN/DOX pre-incubated with free HA.

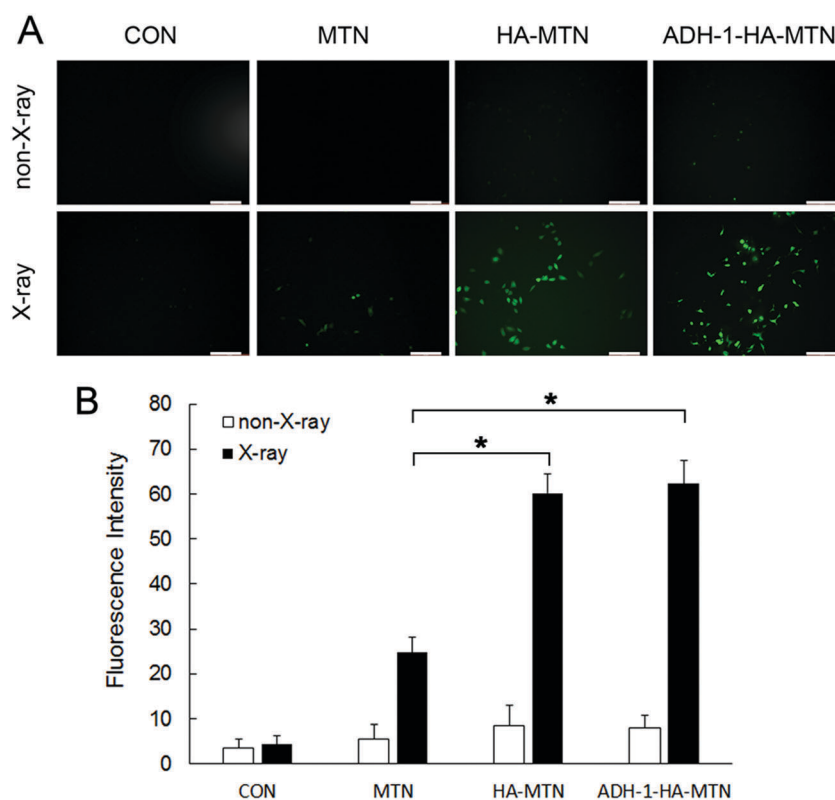


Fig. 7 Intracellular ROS generated by different MTNs under X-ray irradiation. (A) Confocal laser-scanning microscopy images of A549/EMT cells after incubation with nanoparticles in the absence or presence of X-rays by DCFH-DA staining. Scale bars represent 200 μ m. (B) Flow cytometry quantitative results of A549/EMT cells after incubation with nanoparticles in the absence or presence of X-rays by DCFH-DA staining. Data are presented as mean \pm SD ($n = 3$). * $p < 0.05$.

not significantly affect the survival of cells (Fig. S4, ESI[†]). As seen in Fig. 9A, it could be found that ADH-1-HA-MTN/DOX greatly enhanced the killing capacity against resistant tumor cells, and the cytotoxicity of ADH-1-HA-MTN/DOX was further improved under X-ray irradiation. It is reported that EMT results in the suppression of drug transporter and concentrating proteins, contributing to drug resistance.³² Changes in the

protein expressions of the epithelial marker E-cadherin and the mesenchymal marker N-cadherin were analyzed by western blotting. As shown in Fig. 9B, compared with HA-MTN, ADH-1-HA-MTN reduced the N-cadherin expression and increased the E-cadherin expression in A549/EMT cells. This result indicated that ADH-1-HA-MTN overcame the resistance of tumor cells by preventing the EMT process of tumor cells.

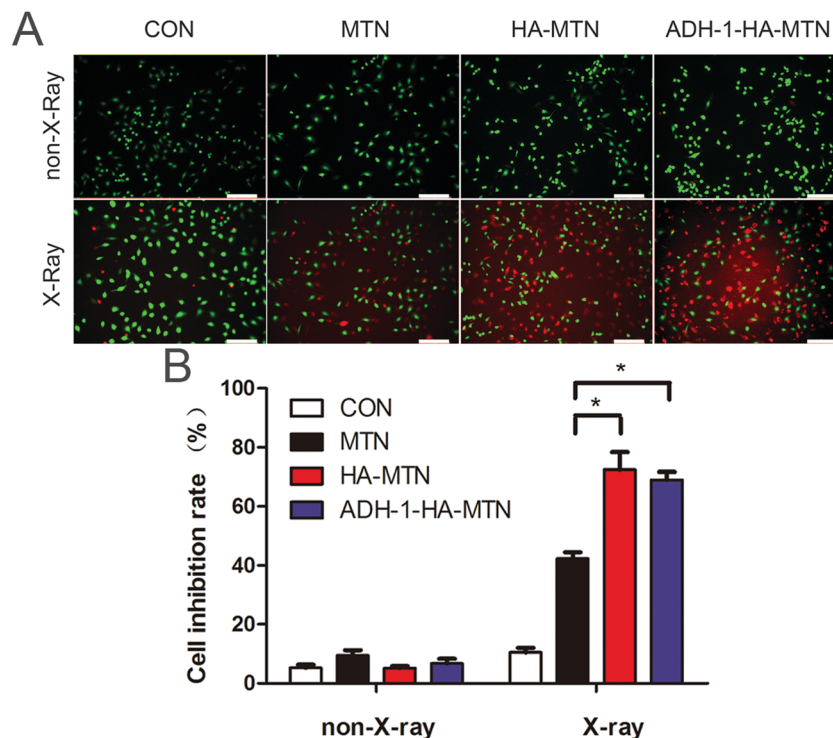


Fig. 8 The therapeutic effect of PDT of different MTNs *in vitro*. (A) Fluorescence images of A549/EMT cells treated with complete RPMI, MTN, HA-MTN or ADH-1-HA-MTN with or without X-ray irradiation. Green: Calcein-AM, live cells; Red: PI, dead cells. Scale bars represent 200 μm. (B) The cell inhibition rate was calculated by counting the live/dead cells using imageJ software ($n = 4$). * $p < 0.05$.

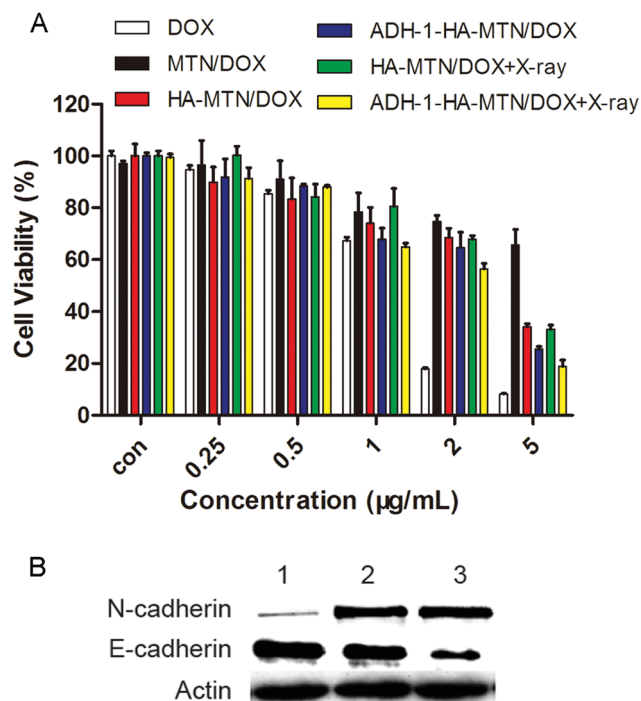


Fig. 9 (A) The *in vitro* cytotoxicity of free DOX, MTN/DOX, HA-MTN/DOX or ADH-1-HA-MTN/DOX with or without X-ray irradiation ($n = 4$). (B) Expression of N-cadherin and E-cadherin in A549/EMT cells treated with (1) ADH-1-HA-MTN, (2) HA-MTN/DOX, and (3) complete RPMI.

Conclusions

In this study, functional mesoporous titanium dioxide nanoparticles with photodynamic effects were successfully synthesized and characterized. After the modification of the MTNs with ADH-1-HA, their average particle size was only about 110 nm. According to *in vitro* studies, ADH-1-HA-MTN/DOX exhibited higher cellular uptake efficiency in A549/EMT cells *via* CD44 receptor-mediated endocytosis. Since the EMT process was prevented by ADH-1, ADH-1-HA-MTN/DOX had stronger cytotoxicity towards tumor cells. In addition, the ROS generated by the nanomaterial itself under X-ray irradiation further improved the killing effect on tumor cells. Undeniably, the results of this study will provide a new strategy for overcoming drug resistance by EMT targeting inhibition combined with photodynamic therapy using the MTN-based drug delivery system.

Conflicts of interest

There are no conflicts to declare.

Acknowledgements

This work was supported by the National Natural Science Foundation of China (81603049, 41504113, and 81760760), the Dalian University of Technology Fundamental Research

Fund (DUT17JC06 and DUT17LK34) and the College Students' Innovative and Entrepreneurial Training Program.

Notes and references

- Z. Guo, W. Li, Y. Yuan, K. Zheng, Y. Tang, K. Ma, C. Cui, L. Wang, B. He and Q. Zhang, *Drug Delivery*, 2018, **25**, 112–121.
- K. Yano, T. Tomono and T. Ogihara, *Biol. Pharm. Bull.*, 2018, **41**, 11–19.
- R. Heery, S. P. Finn, S. Cuffe and S. G. Gray, *Cancers*, 2017, **9**, 38.
- R. Kalluri and E. G. Neilson, *J. Clin. Invest.*, 2003, **112**, 1776–1784.
- R. Kalluri and R. A. Weinberg, *J. Clin. Invest.*, 2009, **119**, 1420–1428.
- J. M. Lee, S. Dedhar, R. Kalluri and E. W. Thompson, *J. Cell Biol.*, 2006, **172**, 973–981.
- J. P. Thiery, H. Acloque, R. Y. Huang and M. A. Nieto, *Cell*, 2009, **139**, 871–890.
- W. Li, Z. Guo, K. Zheng, K. Ma, C. Cui, L. Wang, Y. Yuan and Y. Tang, *Int. J. Pharm.*, 2017, **534**, 71–80.
- C. K. Augustine, Y. Yoshimoto, M. Gupta, P. A. Zipfel, M. A. Selim, P. Febbo, A. M. Pendergast, W. P. Peters and D. S. Tyler, *Cancer Res.*, 2008, **68**, 3777–3784.
- G. Yang, L. Xu, J. Xu, R. Zhang, G. Song, Y. Chao, L. Feng, F. Han, Z. Dong, B. Li and Z. Liu, *Nano Lett.*, 2018, **18**, 2475–2484.
- V. G. Deepagan, D. G. You, W. Um, H. Ko, S. Kwon, K. Y. Choi, G. R. Yi, J. Y. Lee, D. S. Lee, K. Kim, I. C. Kwon and J. H. Park, *Nano Lett.*, 2016, **16**, 6257–6264.
- M. Firczuk, D. Nowis and J. Golab, *Photochem. Photobiol. Sci.*, 2011, **10**, 653–663.
- S. S. Lucky, N. M. Idris, K. Huang, J. Kim, Z. Li, P. S. Thong, R. Xu, K. C. Soo and Y. Zhang, *Theranostics*, 2016, **6**, 1844–1865.
- J. Shi, Z. Chen, B. Wang, L. Wang, T. Lu and Z. Zhang, *ACS Appl. Mater. Interfaces*, 2015, **7**, 28554–28565.
- J. G. Croissant, Y. Fatieiev, A. Almalik and N. M. Khashab, *Adv. Mater.*, 2017, **29**, 1604634.
- Q. Yu, J. Sun, X. Zhu, L. Qiu, M. Xu, S. Liu, J. Ouyang and J. Liu, *J. Mater. Chem. B*, 2017, **5**, 6081–6096.
- Z. Yin, L. Wu, H. Yang and Y. Su, *Phys. Chem. Chem. Phys.*, 2013, **15**, 4844–4858.
- R. Cai, Y. Kubota, T. Shuin, H. Sakai, K. Hashimoto and A. Fujishima, *Cancer Res.*, 1992, **52**, 2346–2348.
- C.-C. Yang, Y.-J. Sun, P.-H. Chung, W.-Y. Chen, W. Swieszkowski, W. Tian and F.-H. Lin, *Ceram. Int.*, 2017, **43**, 12675–12683.
- M. Nakayama, R. Sasaki, C. Ogino, T. Tanaka, K. Morita, M. Umetsu, S. Ohara, Z. Tan, Y. Nishimura, H. Akasaka, K. Sato, C. Numako, S. Takami and A. Kondo, *Radiat. Oncol.*, 2016, **11**, 91.
- M. Gotte and G. W. Yip, *Cancer Res.*, 2006, **66**, 0233–0237.
- S. Liu, G. Han, M. Shu, L. Han and S. Che, *J. Mater. Chem.*, 2010, **20**, 10001–10009.
- J. Liu, B. Zhang, Z. Luo, X. Ding, J. Li, L. Dai, J. Zhou, X. Zhao, J. Ye and K. Cai, *Nanoscale*, 2015, **7**, 3614–3626.
- M. Zhang, C. Xu, L. Wen, M. K. Han, B. Xiao, J. Zhou, Y. Zhang, Z. Zhang, E. Viennois and D. Merlin, *Cancer Res.*, 2016, **76**, 7208–7218.
- J. Choi, V. Reipa, V. M. Hitchins, P. L. Goering and R. A. Malinauskas, *Toxicol. Sci.*, 2011, **123**, 133–143.
- A. N. Ilinskaya and M. A. Dobrovolskaia, *Nanomedicine*, 2013, **8**, 969–981.
- Standard test method for analysis of hemolytic properties of nanoparticles, ASTM E2524-08, ASTM International, Pennsylvania, USA, 2013.
- B. Deng, Q. Y. Tan, R. W. Wang, Y. G. Jiang, J. H. Zhou and W. Huang, *Oncol. Lett.*, 2014, **8**, 454–460.
- S. H. Baek, J. H. Ko, J. H. Lee, C. Kim, H. Lee, D. Nam, J. Lee, S. G. Lee, W. M. Yang, J. Y. Um, G. Sethi and K. S. Ahn, *J. Cell. Physiol.*, 2017, **232**, 346–354.
- H. Ko, H. Jeon, D. Lee, H. K. Choi, K. S. Kang and K. C. Choi, *Bioorg. Med. Chem. Lett.*, 2015, **25**, 5508–5513.
- J. Zhang, Y. Sun, B. Tian, K. Li, L. Wang, Y. Liang and J. Han, *Colloids Surf., B*, 2016, **144**, 293–302.
- X. Zheng, J. L. Carstens, J. Kim, M. Scheible, J. Kaye, H. Sugimoto, C. C. Wu, V. S. LeBleu and R. Kalluri, *Nature*, 2015, **527**, 525–530.